Discover Oncology

Research

LINC00313 promotes the aggressiveness and tumorigenesis of cholangiocarcinoma through targeting miR-320b and MITF

Ziyu Wang[1] · Jiao Li[1] · Jing Xu[1] · Tingqiu Wan[1] · Yunjin Ya[1] · Xi Li[1] · Xi Wang[1] · Yan Jin[1]

Received: 10 December 2024 / Accepted: 23 April 2025
Published online: 07 May 2025

Abstract

Objective Cholangiocarcinoma, a cancer of the biliary duct, is frequently diagnosed in advanced stages with poor prognosis. Understanding the molecular mechanisms driving its progression is crucial for developing effective treatment approaches. This research delves into the role of LINC00313 in regulating the aggressiveness of cholangiocarcinoma cells.
Methods Clinical samples were collected to examine the expression pattern of LINC00313, miR-320b, and MITF using RT-qPCR and western blot analysis. Functional experiments, including cell proliferation, migration, and invasion assays, as well as apoptosis detection, were performed to assess the malignant properties of cholangiocarcinoma cells. The tumorigenic potential of cholangiocarcinoma cells was further investigated in a xenograft mouse model.
Results Elevated levels of LINC00313 were detected in both cholangiocarcinoma tumors and cell lines. Knocking down LINC00313 reduced the aggressiveness of cholangiocarcinoma cells and hindered their ability to form tumors in vivo. It was discovered that miR-320b is a target of LINC00313, exhibiting an expression pattern and functional role that contrasts with LINC00313. Moreover, the LINC00313/miR-320b axis was found to regulate the expression of MITF, thereby influencing the aggressiveness of cholangiocarcinoma cells.
Conclusion LINC00313/miR-320b/MITF axis is implicated in the malignant progression of cholangiocarcinoma, indicating the potential of targeting LINC00313 as a strategy for cholangiocarcinoma clinical management.

Keywords Cholangiocarcinoma · LINC00313 · miR-320b · MITF · Aggressiveness

1 Introduction

Cholangiocarcinoma is a type of cancer that develops in the biliary duct tree of the digestive system. Due to often being detected in advanced stages, the chances of metastasis and cancer recurrence are high, which hinders the effectiveness of treatments such as surgery and chemotherapy [1]. Drug resistance is another common challenge in managing cholangiocarcinoma [2, 3]. Epidemiological studies show that the 5-year survival rate for patients with this cancer is typically between 20 and 30% [4]. The highest number of deaths usually occurs within the first year

Ziyu Wang and Jiao Li: Co-first authors.

Supplementary Information The online version contains supplementary material available at https://doi.org/10.1007/s12672-025-02472-9.

✉ Yan Jin, 13312503258@163.com | [1]Department of Hepatobiliary and Pancreatic Surgery, The First People's Hospital of Yunnan Province, The Affiliated Hospital of Kunming University of Science and Technology, No. 157 Jinbi Road, Xishan District, Kunming 650100, Yunnan, China.

after diagnosis, highlighting the poor prognosis associated with cholangiocarcinoma [5]. There is a global rise in the incidence of this cancer, particularly in developed countries [6, 7]. Early detection and prompt treatment are crucial for improving the survival rates of individuals with cholangiocarcinoma.

Accumulating studies have suggested that long non-coding RNAs (lncRNAs) interact with microRNAs (miRNAs) as the competing endogenous RNAs (ceRNAs) regulate target genes involved in tumor initiation and progression [8, 9]. Dysregulation of lncRNAs plays crucial roles in cell metabolism, growth, and the aggressiveness of tumor cells [10, 11]. The ceRNA regulatory module, comprising lncRNA-miRNA-mRNA interactions, has been implicated in the advancement of various cancers, including gastric, breast, pancreatic, and liver cancer [12–15]. In cholangiocarcinoma, lncRNA AFAP1-AS1 was upregulated to foster the proliferation and mobility of tumor cells [16]. The knockdown of AFAP1-AS1 attenuated the aggressiveness of cholangiocarcinoma cells by arresting cell cycle progression and impairing cell migration. Additionally, overexpression of lncRNA CCAT1 has been shown to enhance the malignant characteristics of cholangiocarcinoma cells by downregulating miR-152 expression [17]. Recent findings also suggest that the aberrant overexpression of lncRNA ANRIL and lncRNA SNHG3 sustain the malignancy of cholangiocarcinoma cells by targeting different miRNAs [18, 19]. Therefore, understanding the comprehensive ceRNA network in cholangiocarcinoma progression is essential not only for identifying markers of malignant progression but also for pinpointing potential therapeutic targets.

Current research has identified various ceRNA modules involving differentially expressed lncRNAs and miRNAs in cholangiocarcinoma progression [20, 21]. However, the specific functional roles of these non-coding RNAs in regulating malignant characteristics in cholangiocarcinoma cells are still not well understood. Among several dysregulated lncRNAs, LINC00313 was identified as one of the most significantly upregulated transcripts in cholangiocarcinoma samples compared to normal tissues [21]. Our clinical validation confirmed this upregulation pattern, and given its unexplored functional role in cholangiocarcinoma progression, we selected LINC00313 for detailed mechanistic investigation. This study aims to investigate the expression pattern of LINC00313 in cholangiocarcinoma clinical samples, explore its impact on the aggressive features of cholangiocarcinoma cells, and investigate in vivo tumorigenesis after LINC00313 knockdown. Functional interaction experiments were conducted to identify the downstream targets responsible for the biological functions of LINC00313.

2 Methods and materials

2.1 Clinical sample collection

In this study, we collected the tumor specimens and the matched para-cancerous samples by surgery from 14 patients diagnosed with cholangiocarcinoma at First People's Hospital of Yunnan Province. The study included 14 pairs of cholangiocarcinoma tissues and adjacent normal tissues. Among these patients, 8 were male and 6 were female, with a median age of 54 years (range: 41–54 years). Based on the TNM staging system, 5 patients were classified as stage II, 7 as stage III, and 2 as stage IV. Histologically, 9 cases were moderately differentiated and 5 were poorly differentiated. Cholangiocarcinoma was confirmed through histological examination of the tumor samples by two independent pathologists from the Department of Pathology. Inclusion criteria: patients diagnosed with primary cholangiocarcinoma without medical record of chronic diseases. Exclusion criteria: patients who were diagnosed with other cancers, or patients who had undergone preoperative radiotherapy, chemotherapy or hormone drug administration. The clinical samples were stored in − 80 °C freezer until further analyses. The enrolled individuals in the study signed the informed written letter of consent. The use of human samples gained the approval of the Medical Ethics Committee of First People's Hospital of Yunnan Province. The parents of all the recruited subjects signed the informed consent.

2.2 Cell culture and the generation of stable LINC00313 knockdown cell line

Human intrahepatic biliary epithelial cells (HIBEpiC) (Cat# YB-ATCC-8492, Shanghai Yubo Biological Technology Co., Ltd., Shanghai, China), cholangiocarcinoma cell lines [CCLP1 (Cat# AE-886, Shanghai Yubo Biological Technology Co., Ltd., Shanghai, China), SG231 (Cat# SG231-001, Shanghai Guandao Bioengineering Co., Ltd., Shanghai, China), HuCCT1 (Cat# CL-0725, Wuhan Procell Life Science & Technology Co., Ltd., Wuhan, China)], and human embryonic kidney cell line [HEK293 cells (Cat# CL-0001, Wuhan Procell Life Science & Technology Co., Ltd., Wuhan, China)] were cultivated with

DMEM medium (GE™ Hyclone, Utah, U.S.) containing 10% FBS (GE™ Hyclone, Utah, U.S.), 100 U/ml penicillin and 100 mg/ml streptomycin (Procell, Wuhan, China) in a humidified atmosphere of 37 °C and 5% CO2. HuCCT1 cells with stable LINC00313 knockdown were generated using the lentiviral system carrying shRNA targeting LINC00313. Briefly, a combination of pSPAX2/pMD2.g (packaging vectors) and PCDH-sh-Ctrl-puro (control virus vector) or PCDH-sh-LINC00313-puro (knockdown virus plasmid) (GenePharma, Shanghai, China) were co-transfected into HEK293 cells using Lipofectamine 3000 (Invirtogen, Shanghai, China). 48 h post transfection, the cell culture supernatant containing the lentiviral particles was collected to infect HuCCT1 cells in the presence of polybrene (8 g/mL, Beyotime, Beijing, China). Uninfected cells were eliminated with 1 g/ml puromycin (Beyotime, Beijing, China) for 14 days. HuCCT1 cells carrying sh-Ctrl or sh-LINC00313 were maintained in the complete medium with 0.5 g/ml puromycin.

2.3 Cell transfection

The oligos of miR-NC, miRNA mimic, inhibitor NC and miRNA inhibitor were purchased from RiboBio L.T.D. (Guangzhou, China). The empty vector (pcDNA3.1 empty vector) and MITF expression plasmid (pcRNA3.1-MITF) were produced by GenePhama (Shanghai, China). The oligos and plasmids were transfected into HuCCT1 cells using Lipofectamine 3000 (Invirtogen, Shanghai, China) based on the supplier's protocols. 48 h after the transfection, cells were harvested for functional experiments (Additional file 1).

2.4 Animals and the xenograft model

The animal experimental protocols were approved by the Experimental Animal Ethics Committee of Yunnan Besta Biotechnology Co. LTD.(BST-MICE-20221229-02). Ten 8-week-old (weighed 25–35 g) Balb/C nude mice acquired from Beijing Vital River Laboratory Animal Technology Co., Ltd. (Beijing, China) were raised in the standard SPF animal facility with 60%-65% humidity and an 12 h light/dark cycle at 22 °C. The mice were randomly assigned into two experimental groups (n = 5 animals in each group): the sh-NC group (subcutaneously injected with 1×10^6 HuCCT1 cells carrying sh-Ctrl sequence after lentivirus infection) and sh-LINC00313 group (injected with 1×10^6 cells carrying sh-LINC00313 sequence after lentivirus infection). Tumor volume was recorded every week using a caliper based on the formula: V(tumor) = 0.5 × length × width^2 (mm3). 35 days after tumor cell inoculation, all the mice were euthanized by cervical dislocation. The xenogfart tumor samples were collected for subsequent analyses.

2.5 Real-time quantitative PCR (RT-qPCR)

Total RNA samples from cultured cells (1×10^6) and tissue samples (5 mg) were extracted using Trizol reagent (Beyotime Biotechnology, Beijing, China). Afterward 1 μg of total RNA sample was reverse transcribed into cDNA using BeyoRT™II First Strand cDNA Synthesis Kit (Beyotime Biotechnology, Shanghai, China) or microRNA Reverse Transcription Kit (EZB-miRT2) (Ezbioscience, MN, USA). The TB Green® Fast qPCR Mix (Takara Biomedical Technology (Beijing) Co., Ltd., Beijing, China) was used to perform the real-time qPCR analysis. The following PCR cycling conditions were used: 95 °C 2 min for initial denaturation, 40 cycles of 95 °C 30 s denaturation, 60 °C 30 s annealing and 72 °C 60 s extension. Finally, the $2^{-\Delta\Delta Ct}$ method was used to analyze the relative expression level, with GAPDH and U6 snRNA as internal references. qPCR primer sequences were listed in Additional file 2: Table S1.

2.6 Western blot (WB)

Total protein samples were extracted from tissues (10 mg) and cells (1×10^6) using RIPA lysis buffer containing protease inhibitor cocktail (Zeye Biotech, Shanghai, China). The protein concentration in the cell lysate was measured by a BCA Protein Assay Kit (Beyotime Biotech, Beijing, China). Afterward 10 □g protein of each group was subjected to SDS–polyacrylamide gel electrophoresis, and the protein bands were transferred to the PVDF membrane. The membrane was blocked with 5% milk at room temperature for 1 h, followed by the incubation with the corresponding primary antibodies (Abcam, Cambridge, UK) overnight at 4 °C: anti-Bcl-2 (ab59348, 1: 1000), anti-Bax (ab53154, 1:1000); anti-Cleaved Caspase-3 (ab2302, 1:1000), anti-actin (ab8227, 1:1000), PARP-1 (ab227244, 1: 1000), cleaved PARP-1 (ab4830, 1: 1000) and anti-MITF (ab12039, 1:1000). After washing the membrane was further probed with HRP-linked secondary antibody (1:3000; Cell Signaling Technologies #7074, MA, USA) for 1 h. The signal development was conducted using an enhanced

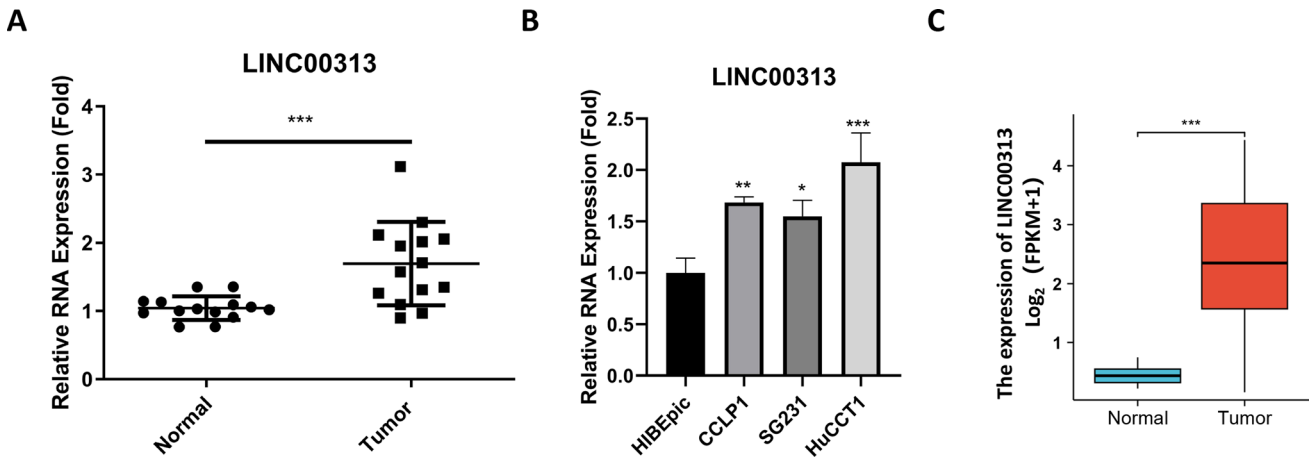

Fig. 1 LINC00313 upregulation in cholangiocarcinoma tumor and cell lines. **A** RT-qPCR analysis of LINC00313 levels in 14 pairs of cholangiocarcinoma tumor specimens and the para-cancerous normal samples. **B** Examination of LINC00313 levels in human intrahepatic biliary epithelial cells (HIBEpiC) and cholangiocarcinoma cell lines (CCLP1, SG231, HuCCT1) by RT-qPCR. n = 3 independent experiments. **C** Analysis of LINC00313 levels in normal and tumor samples of TCGA cholangiocarcinoma cohort. *$p < 0.05$; **$p < 0.01$; ***$p < 0.001$

chemiluminescence kit (Santa Cruz, TX, USA,) and the protein bands were visualized on a gel imaging system (Bio-Rad, Hercules, CA, United States).

2.7 Apoptosis detection by flow cytometry

HuCCT1 cells were trypsinized and washed twice with PBS, and re-suspended in the Annexin V binding buffer. The analysis of apoptotic events was performed using the FITC Annexin V Apoptosis Detection Kit (BD Biosciences, MA, USA). Briefly, 1 µL Annexin V-FITC and 1 µL Propidium-Iodide reagent were mixed with 1×10^6 cells for 15 min incubation in the darkness. After staining the cells were centrifuged and washed twice with the binding buffer without dyes. The quantification of apoptotic cells was conducted on a FACS Calibur cytometer with CellQuest Pro software (BD Biosciences). For compensation and gating purposes, we included unstained cells, single-stained controls (Annexin V-FITC only and PI only), and a positive control (cells treated with 1 µM staurosporine for 24h to induce apoptosis) to ensure accurate discrimination between early apoptotic and late apoptotic/necrotic cell populations.

2.8 Luciferase reporter assay

The prediction of interacting sequences between lncRNA/miRNAs and miRNA/mRNA was perfromed using "Targetscan" online resources (http://www.targetscan.org/miRanda). Afterward the wild-type or mutated binding sites were cloned into the pKC-4.04 luciferase reporter (Addgene, MA, USA). The reporter with wild-type or mutated sequences was co-transfected into HEK293 cells with miRNA mimic or miR-NC for 48 h. The luciferase activities were measured by the Fire-Lumi™ Dual Luciferase Assay Kit (Nanjing GenScript Biotechnology Co., Ltd., Nanjing, China). After the cell lysates (100 µL) were transferred to an opaque-walled 96-well plate, 50 µL of the Luciferase Assay Reagent II (LAR II) was added to each well. The contents in each well were gently mixed by pipetting up and down. Data were recorded using SpectraMax iD3 multi-mode microplate reader (Molecular Devices, Sunnyvale, CA, USA). The firefly luciferase activity in each well was measured by recording the luminescence values at a wavelength of 560 nm. Subsequently, 50 µL of the Stop & Glo Reagent was added to each well, and the Renilla luciferase activity was determined by recording the luminescence values at a wavelength of 480 nm.

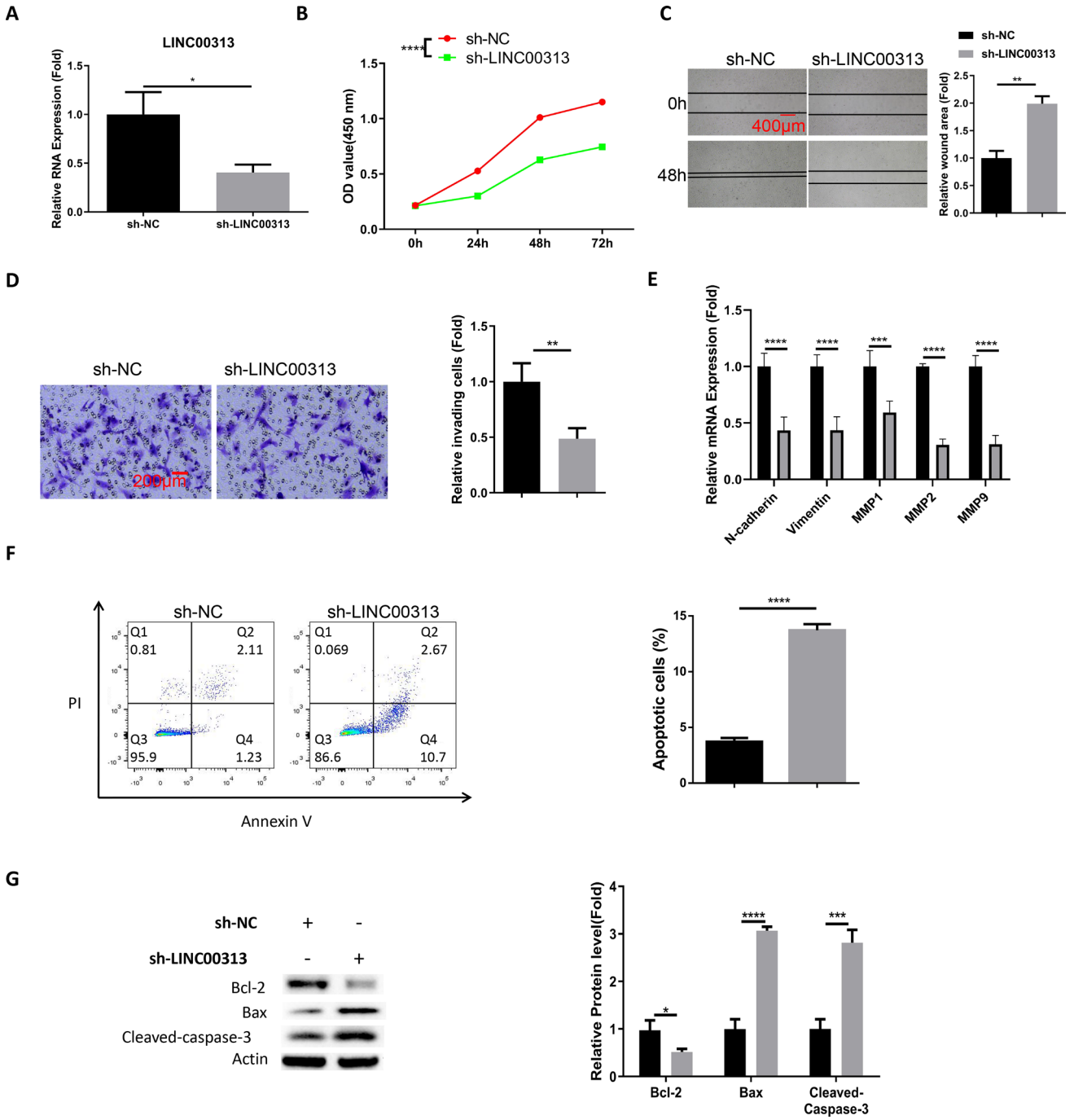

Fig. 2 Targeting LINC00313 impairs the aggressiveness of cholangiocarcinoma cells. HuCCT1 cells were infected with lentivrius to stably express control shRNA (sh-Ctrl) and the shRNA targeting LINC00313 (sh-LINC00313). **A** RT-qPCR analysis of LINC00313 expression in sh-Ctrl and sh-LINC00313 groups. **B** CCK-8 proliferation assay, **C** Wound healing migration assay, **D** Transwell invasion assay, **E** RT-qPCR detection of N-cadherin, Vimentin, MMP1, MMP2, and MMP9, **F** Apoptosis detection by flow cytometry, and **G** WB analysis of apoptosis-related proteins (Bax, cleaved caspase-3, and Bcl-2) in sh-Ctrl and sh-LINC00313 group. n = 3 independent experiments. *$p < 0.05$; **$p < 0.01$; ***$p < 0.001$; ****$p < 0.0001$

2.9 CCK-8 proliferation assay

HuCCT1 cells with different treatment were seeded in to a 96-well plate at 2000 cells/well and the cells were allowed to grow for different time period. Accordingly, 10 μL CCK8 reagent (Solarbio, Beijing, China) was added to the cell culture

A

miRDB		TargetScan	
miRNA	Score	miRNA	Score
miR-320b	95	miR-320b	82
miR-195-5p	84	miR-4229	15
miR-199a-5p	68	miR-218-5p	75
miR-4229	72	miR-525-5p	36
miR-218-5p	83	miR-342-3p	42
miR-525-5p	36	miR-422a	75
miR-342-3p	68		
miR-422a	59		

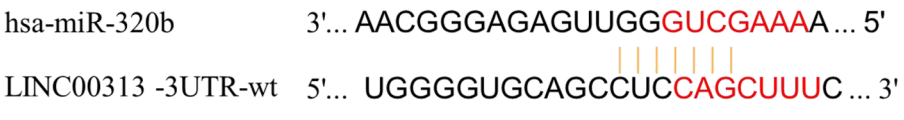

B

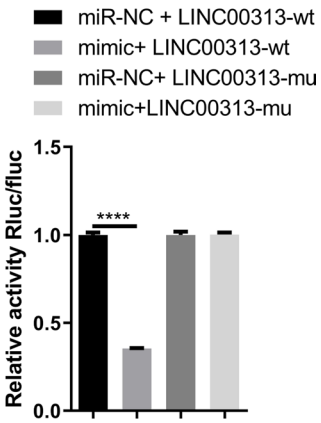

C

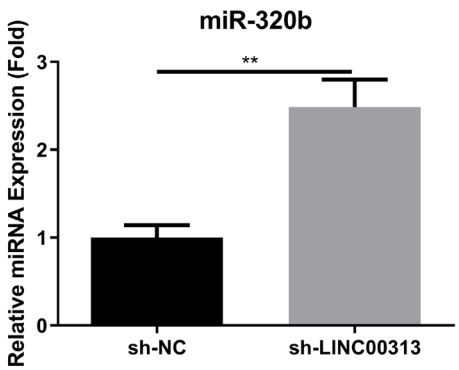

D

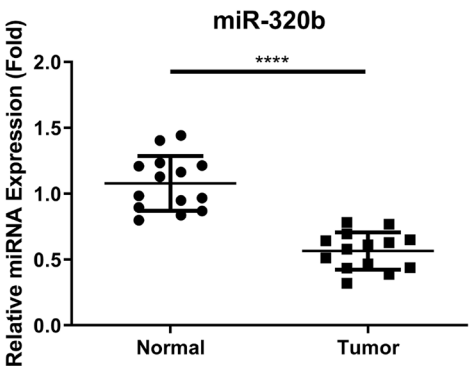

Fig. 3 miR-320b is a candidate target of LINC00313. **A** The prediction of interacting sites between LINC00313 and miR-320b using Targetscan online database. **B** Dual luciferase assay using wild-type (WT) or mutated (MUT) reporters in HEK293 cells. **C** RT-qPCR analysis of miR-320b expression in sh-Ctrl and sh-LINC00313 groups. **D** RT-qPCR analysis of miR-320b levels in 14 pairs of cholangiocarcinoma tumor specimens and the para-cancerous normal samples. n = 3 independent experiments. $^{**}p < 0.01$; $^{****}p < 0.0001$

for 3 h in the cell culture incubator. The absorbance value (OD value) in each well was measured at 450 nm wavelength on a Synergy H1 microplate reader (Winooski, Vermont, USA).

2.10 Transwell chamber assay

Transwell cassette (Corning, NY, USA) with the 8 μm pore size was used as the physical barrier for the invasion assay, and the upper chamber was coated with Matrigel (BD Biosciences, Bedford, USA) to mimic the extracellular matrix during tissue invasion. HuCCT1 cells were trypsinized and collected in serum-free medium. The cells were inoculated in the upper chamber at a cell density of 5×10^5 cells/ml. The lower compartment was filled with 600 μl of complete medium with 20% FBS. After 24 h, cells on the Transwell membrane were fixed and stained with 0.1% crystal violet (Sigma, Shanghai, China) for 20 min. The invading cells on the membrane were quantified under a light microscope at 100× magnification. For each sample, 5 random fields were counted using Leica AM6000 microscope (Leica, Wetzlar, Germany).

2.11 Wound-healing assay

HuCCT1 cells were plated in 6 well plates and the cells were allowed to reach about 80–90% confluence. A scratch wound was generated in the central region of the cell monolayer using a sterile pipette tip. The floating cells were removed by replenishing the fresh medium. The remaining cells were cultured at 37 °C for 24–48 h. Cell images were recorded using an inverted light microscope (Leica AM6000 microscope).

2.12 Immunohistochemical (IHC) staining

Xenograft tumor samples were collected from the mice and fixed in 10% PFA for 12h. The staining was performed in 5-μm sections of formalin-fixed paraffin-embedded (FFPE) tissues. The sections were initially deparaffinized and re-hydrated. The antigen unmasking was achieved by heating the sections in the citrate antigen recovery solution (Beyotime, Beijing, China) at 95 °C for 5 min. The peroxidase activity in the sections was quenched by 3% hydrogen peroxide for 10 min. After the rinsing in TBST buffer, the sections were blocked for 1 h with 5% normal goat serum. The primary antibody against Ki-67 (ab15580, 1:500, Abcam, Cambridge, UK) was used to label the sections overnight. After washing by TBST buffer, the sections were further labeled in the SignalStain® Boost Detection Reagent (HRP, Rabbit #8114, Cell Signaling Technologies, MA, USA) for 30 min at room temperature. The sample was observed under the Leica AM6000 microscope (Leica, Wetzlar, Germany).

2.13 Statistical analysis

The results presented in the study were summarized as the mean ± SD of three independent trials. The researchers were blinded to treatment or control groups when performing data analysis and collection. The difference between two condition was compared by unpaired student's t test. The analyses of multiple conditions were conducted by one-way analysis of variance (ANOVA) and Tukey's post-hoc test. Data at multiple time points were compared using two-way ANOVA. Data were deemed statistically significant when the P value was less than 0.05.

3 Results

3.1 LINC00313 upregulation in cholangiocarcinoma tumor and cell lines

We initially collected 14 pairs of cholangiocarcinoma tumor specimens and para-cancerous normal samples to examine LINC00313 expression pattern. It was found that LINC00313 displayed a significant upregulation in tumor samples compared to the normal counterparts (Fig. 1a). Examination of LINC00313 levels in human intrahepatic biliary epithelial cells (HIBEpiC) and cholangiocarcinoma cell lines (CCLP1, SG231, HuCCT1) further demonstrated the overexpression of LINC00313 in cholangiocarcinoma cell lines (Fig. 1b). We also analyzed the TCGA cholangiocarcinoma cohort to validate our findings. Analysis of LINC00313 expression in this dataset revealed that LINC00313 was significantly upregulated in cholangiocarcinoma tissues compared to normal tissues (Fig. 1c).

3.2 Targeting LINC00313 impairs the aggressiveness of cholangiocarcinoma cells

Given that HuCCT1 cells demonstrated the highest endogenous expression levels of LINC00313 among the three CCA cell lines tested, making it a suitable model for shRNA-based loss-of-function analysis, we selected this cell line for our functional experiments. To understand the biological role of LINC00313 in cholangiocarcinoma cells, we applied lentivirus to stably express control shRNA (sh-Ctrl) and the shRNA targeting LINC00313 (sh-LINC00313) in HuCCT1 cells. sh-LINC00313 group showed a significant reduction of LINC00313 expression compared to the sh-NC group (Fig. 2a). Upon LINC00313 silencing, the aggressiveness of HuCCT1 cells was significantly attenuated, as evidenced by the retarded cell growth ability (Fig. 2b), the impaired cell migration (Fig. 2c) and invasion (Fig. 2d). Consistently, qPCR analysis revealed that knockdown of LINC00313 significantly decreased the expression of invasion-related markers including N-cadherin, Vimentin, MMP1, MMP2, and MMP9 (Fig. 2e). Besides, apoptosis detection by flow cytometry revealed an observable

Fig. 4 LINC00313/miR-320b axis modulates the aggressiveness of cholangiocarcinoma cells. HuCCT1 cells with LINC00313 knockdown were transfected with the synthetic miR-320b inhibitor or the inhibitor control. **A** RT-qPCR analysis of miR-320b expression. **B** CCK-8 proliferation assay, **C** Wound healing migration assay, **D** Transwell invasion assay, **E** RT-qPCR detection of N-cadherin, Vimentin, MMP1, MMP2, and MMP9, **F** Apoptosis detection by flow cytometry, and **G** WB analysis of apoptosis-related proteins (Bax, cleaved caspase-3, and Bcl-2) in each experimental condition. n = 3 independent experiments. *$p < 0.05$; **$p < 0.01$; ***$p < 0.001$; ****$p < 0.0001$

increase of apoptotic events in HuCCT1 cells after LINC00313 silencing (Fig. 2f). WB analysis of apoptosis-related proteins showed increased levels of pro-apoptotic proteins (Bax and cleaved caspase-3) and a lowered level of anti-apoptotic protein (Bcl-2) upon LINC00313 knockdown (Fig. 2g). Therefore, knocking down LINC00313 curtails the malignancy of cholangiocarcinoma cells.

3.3 miR-320b is a candidate target of LINC00313

To elucidate the molecular mechanisms by which LINC00313 promotes cholangiocarcinoma progression, we sought to identify potential microRNA targets of LINC00313. Through bioinformatic analysis using multiple databases including miRDB and TargetScan, miR-320b emerged as a common predicted target with a high score and complementary binding sequences to LINC00313, as shown in Fig. 3a. While other candidates may also mediate the efefcts of LINC00313, we focused on miR-320b due to its consistent prediction across databases and its previously unreported role in cholangiocarcinoma, suggesting a novel regulatory axis in this cancer type. Wild-type (WT) or mutated (MUT) interacting sequences were incorporated into the luciferase reporter to verify the interaction (Fig. 3a). Transfection of miR-320b mimic resulted in a repression of WT luciferase reporter activity, while mutation of the binding sequences nullified this effect (Fig. 3b). Knocking down LINC00313 in HuCCT1 cells led to an increase in miR-320b expression (Fig. 3c). In contrast to the upregulation of LINC00313, miR-320b was significantly downregulated in the cholangiocarcinoma samples compared to normal counterparts (Fig. 3d). These findings indicate that miR-320b is negatively regulated by LINC00313 in cholangiocarcinoma.

3.4 LINC00313/miR-320b axis modulates the aggressiveness of cholangiocarcinoma cells

To investigate the role of miR-320b in the biological function of LINC00313, HuCCT1 cells with LINC00313 knockdown were transfected with either a synthetic miR-320b inhibitor or an inhibitor control. The results showed that miR-320b inhibitor significantly reduced miR-320b levels in HuCCT1 cells with LINC00313 knockdown (Fig. 4a). Subsequent CCK-8 proliferation assay indicated that miR-320b inhibition rescued cell growth following LINC00313 knockdown (Fig. 4b). Moreover, the migratory and invasive capacities of HuCCT1 cells in the sh-LINC00313 group were enhanced after transfection with the miR-320b inhibitor (Fig. 4c, d). Consistent with these findings, qPCR analysis showed that miR-320b inhibition reversed the LINC00313 silencing-induced downregulation of invasion-related markers including N-cadherin, Vimentin, MMP1, MMP2, and MMP9 (Fig. 4e). Analysis of apoptotic events and apoptosis-related factors further demonstrated that miR-320b inhibition suppressed apoptotic cell death induced by LINC00313 silencing in HuCCT1 cells (Fig. 4f, g). Therefore, miR-320b acts as a downstream mediator of LINC00313 in regulating the aggressive phenotype of cholangiocarcinoma cells.

3.5 Melanocyte inducing transcription factor (MITF) is negative targeted by miR-320b

To identify potential downstream targets of miR-320b, we performed comprehensive bioinformatics analysis using three independent miRNA target prediction databases: TargetScan, miRanda, and RNAhybrid. Through this systematic screening approach, we identified MITF as a potential target gene of miR-320b, as all three prediction tools consistently identified potential binding sites for miR-320b in the 3' untranslated region (UTR) of MITF mRNA. As shown in Fig. 5a, sequence alignment revealed that the 3' UTR of MITF mRNA contains conserved complementary binding sites for miR-320b. The luciferase reporter assay showed that miR-320b mimic was able to inhibit the activity of WT reporter containing the predicted interacting sequences, and no inhibition was observed for the reporter containing mutated binding sites (Fig. 5b). Further, miR-320b overexpression by the transfection of

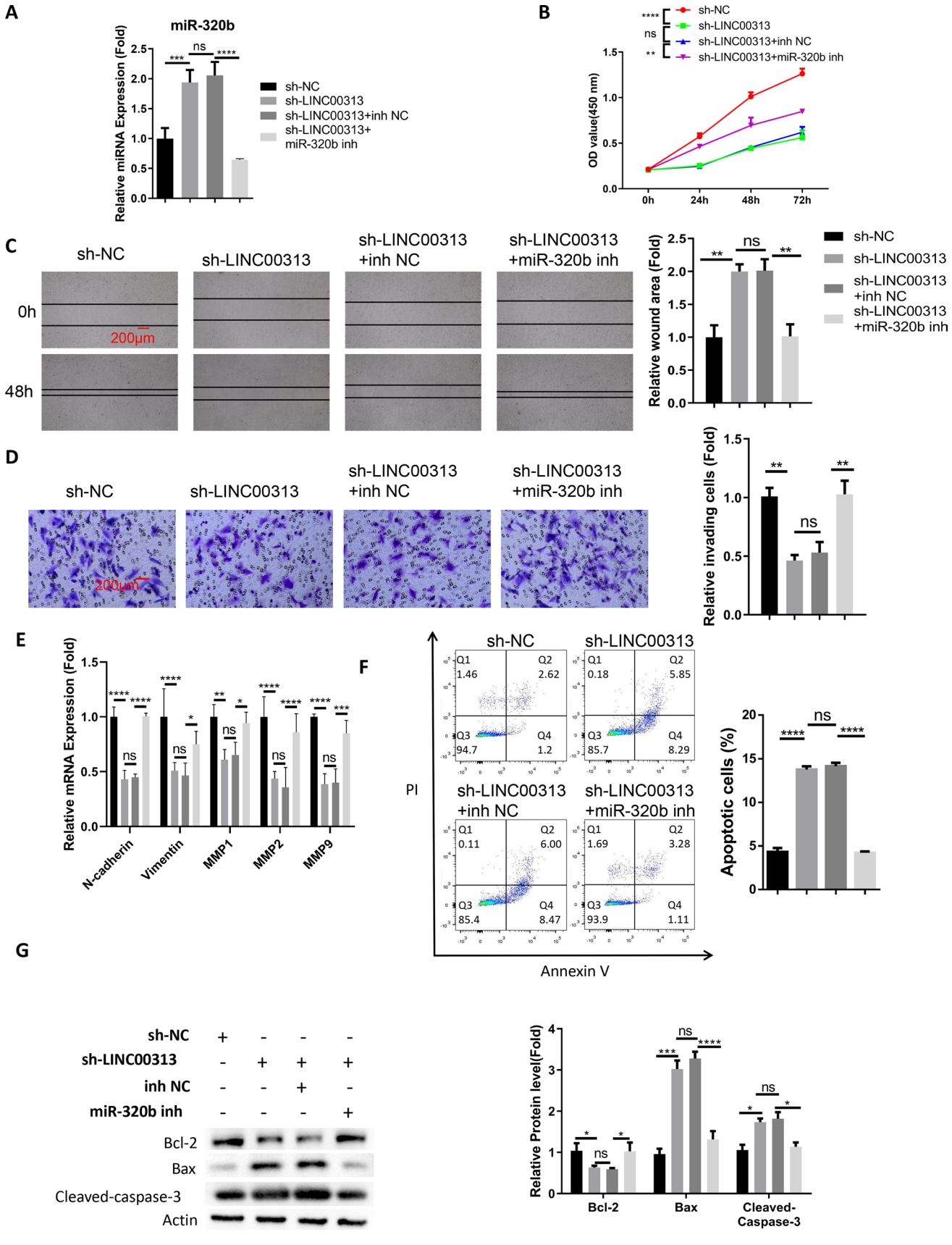
A
miR-320b
Relative miRNA Expression (Fold)
sh-NC
sh-LINC00313
sh-LINC00313+inh NC
sh-LINC00313+ miR-320b inh
B
sh-NC
sh-LINC00313
sh-LINC00313+inh NC
sh-LINC00313+miR-320b inh
OD value(450 nm)
0h
24h
48h
72h
C
sh-NC
sh-LINC00313
sh-LINC00313 +inh NC
sh-LINC00313 +miR-320b inh
0h
48h
200μm
Relative wound area (Fold)
D
sh-NC
sh-LINC00313
sh-LINC00313 +inh NC
sh-LINC00313 +miR-320b inh
200μm
Relative invading cells (Fold)
E
Relative mRNA Expression (Fold)
N-cadherin
Vimentin
MMP1
MMP2
MMP9
F
sh-NC
sh-LINC00313
sh-LINC00313 +inh NC
sh-LINC00313 +miR-320b inh
PI
Annexin V
Apoptotic cells (%)
G
sh-NC
sh-LINC00313
inh NC
miR-320b inh
Bcl-2
Bax
Cleaved-caspase-3
Actin
Relative Protein level(Fold)
Bcl-2
Bax
Cleaved-Caspase-3

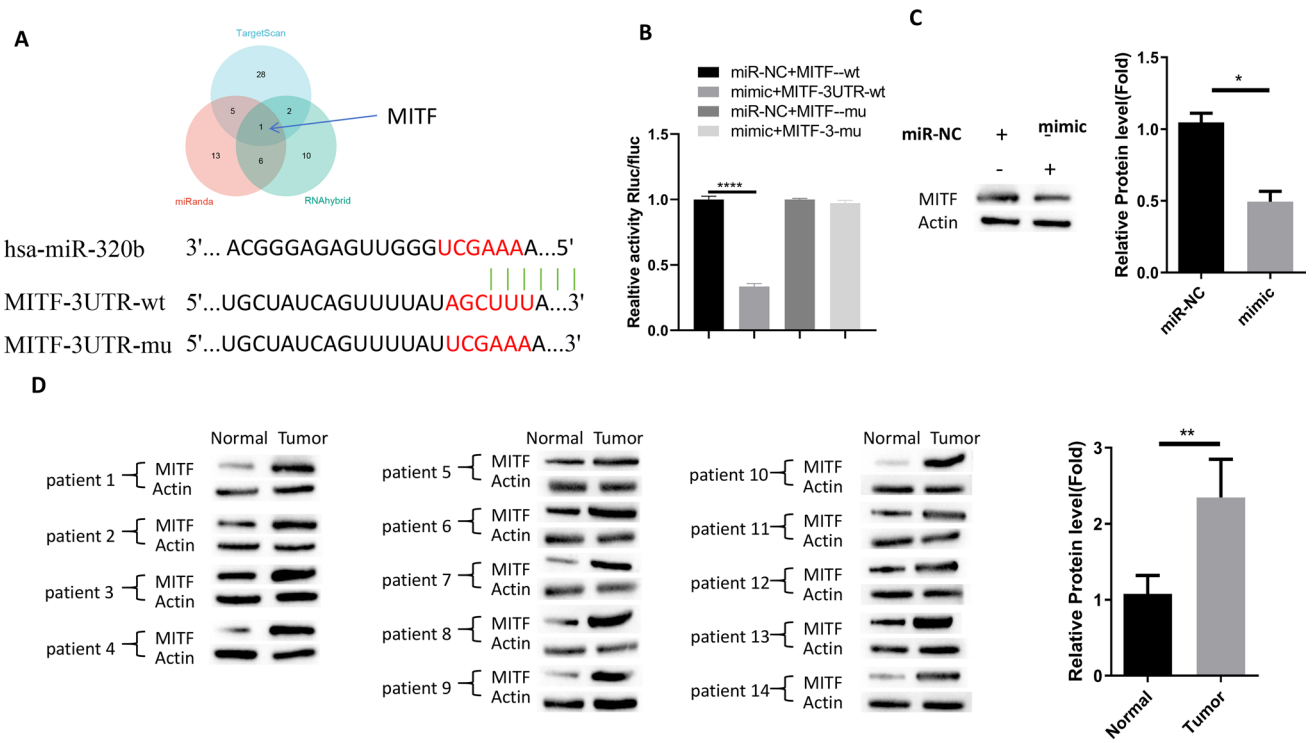

Fig. 5 MITF is negative targeted by miR-320b. **A** The prediction of interacting sites between MITF mRNA and miR-320b using Targetscan online database. **B** Dual luciferase assay using wild-type (WT) or mutated (MUT) reporters in HEK293 cells. **C** WB analysis of MITF protein levels in HuCCT1 cells upon the transfection of miR-320b mimic or miR-NC. **D** WB analysis of MITF protein levels in 14 pairs of cholangiocarcinoma tumor specimens and the para-cancerous normal samples. n = 3 independent experiments. *$p < 0.05$; **$p < 0.01$

miR-320b mimic suppressed MITF protein levels in HuCCT1 cells (Fig. 5c). We also detected MITF protein levels in the clinical samples, and the data showed that MITF levels were significantly elevated in cholangiocarcinoma samples when compared to the normal tissues (Fig. 5d). This is in contrast to the downregulation of miR-320b in cholangiocarcinoma samples, which suggests a regulatory effect of miR-320b on MITF expression.

3.6 MITF overexpression counteracts the effect of miR-320b mimic in HuCCT1 cells

To further dissect the functional interaction between miR-320b and MITF, HuCCT1 cells were transfected with different combinations of miR-NC, miR-320b mimic, empty vector, and MITF expression vector. Overexpression of miR-320b reduced MITF protein levels and co-transfection with MITF expression vector restored MITF expression (Fig. 6a). Similar to the effect of LINC00313 silencing, miR-320b mimic impaired the cell growth, and MITF overexpression largely rescued this effect (Fig. 6b). The migratory and invasive abilities of HuCCT1 cells were also reduced by miR-320b mimic, while MITF overexpression promoted cell migration and invasion (Fig. 6c, d). In line with these observations, qPCR analysis revealed that miR-320b mimic decreased the expression of invasion-related markers (N-cadherin, Vimentin, MMP1, MMP2, and MMP9), while MITF overexpression reversed these changes (Fig. 6e). Furthermore, miR-320b overexpression led to an increase in apoptotic cell death in HuCCT1 cells, which was attenuated by MITF overexpression (Fig. 6f, g). These results support the notion that the inhibitory effect of miR-320b in cholangiocarcinoma cells is mediated by the downregulation of MITF.

3.7 LINC00313 silencing impairs the tumor formation of HuCCT1 cells in nude mice

We next attempted to examine the impact of LINC00313 silencing in a mouse model of xenograft tumor formation. Nude mice were assigned as the sh-NC group (injected with HuCCT1 cells carrying control shRNA) and sh-LINC00313 group (injected with cells carrying LINC00313 shRNA). Tumor growth of HuCCT1 cells was significantly

repressed upon LINC00313 knockdown in vivo, as revealed by the reduction of tumor weight (Fig. 7a). LINC00313 knockdown was associated with an upregulation of miR-320b and a downregulation of MITF in tumor samples (Fig. 7b). The analysis of apoptosis-related factors indicated that LINC00313 knockdown caused an increase of pro-apoptotic proteins (Bax and cleaved caspase-3) in the xenograft tumor samples, as well as the cleavage of PARP-1; while the expression level of anti-apoptotic factor (Bcl-2) was reduced (Fig. 7c). Furthermore, IHC staining showed a nearly twofold reduction of proliferating cells with Ki-67 positive staining in the tumor samples with LINC00313 knockdown (Fig. 7d). Collectively, these data suggest that LINC00313 acts as an oncogenic factor for the malignant progression of cholangiocarcinoma.

3.8 Clinical significance of LINC00313/miR-320b/MITF axis in cholangiocarcinoma patients

To investigate the clinical relevance of the LINC00313/miR-320b/MITF axis, we analyzed their expression patterns and correlation with patient survival using TCGA datasets. As shown in Fig. 8, Kaplan–Meier analysis revealed that patients with high LINC00313 expression exhibited significantly shorter overall survival compared to those with low expression. Conversely, patients with high miR-320b expression showed better overall survival than those with low expression. Furthermore, high MITF expression was associated with poor overall survival. These survival analyses support our experimental findings and suggest that the LINC00313/miR-320b/MITF axis plays a crucial role in cholangiocarcinoma progression and may serve as a potential prognostic biomarker.

4 Discussion

The study demonstrated the overexpression of LINC00313 in cholangiocarcinoma tumor samples and cell lines, which is linked to the malignant phenotype of cholangiocarcinoma cells. Silencing LINC00313 reduced the aggressiveness of cholangiocarcinoma cells and hindered tumorigenesis in vivo. Additionally, it was found that miR-320b is a potential target of LINC00313, exhibiting an expression pattern opposite to that of LINC00313. Overexpression of miR-320b also inhibited the aggressive behavior of cholangiocarcinoma cells. Furthermore, the LINC00313/miR-320b axis influenced the expression of MITF, thereby influencing the aggressiveness of cholangiocarcinoma cells.

LINC00313 has been identified as upregulated in various malignancies, such as testicular germ cell tumors where its overexpression promotes metastasis through the facilitation of epithelial-mesenchymal transition [22]. In cervical cancer, upregulated LINC00313 facilitates tumor progression by accelerating cell cycle progression via the inhibition of miR-4677-3p and upregulation of cyclin-dependent kinase 6 (CDK6) [23] Additionally, LINC00313 enhances malignancy and metastasis of osteosarcoma by interacting with EZH2 mRNA, thereby increasing its stability and promoting EZH2-mediated PTEN suppression [24]. Notably, tumor-derived exosomal LINC00313 has been shown to induce a shift of macrophages towards a M2-like phenotype in non-small cell lung cancer, potentially contributing to an immunosuppressive tumor microenvironment [25]. These findings collectively support the oncogenic role of LINC00313 across different cancer types. Our study further corroborates this by demonstrating LINC00313 overexpression in cholangiocarcinoma, with knockdown of LINC00313 leading to reduced cell proliferation and mobility. Our results align with a previous report of LINC00313 upregulation in cholangiocarcinoma through sequencing analysis [21]. However, There is also inconsistency in LINC00313's biological functions reported across various cancer types and cellular contexts. In osteosarcoma, LINC00313 acts as an oncogene by sponging miR-342-3p to regulate FOSL2 [26], while in chondrocytes, it promotes proliferation through the miR-525-5p/GDF5 axis [27]. These apparently contradictory functions of LINC00313 across different studies likely reflect the context-dependent nature of lncRNA function, which can vary based on cancer type, cellular context, and downstream miRNA targets. This tissue-specific regulation emphasizes the importance of characterizing lncRNA function in each cancer type individually, as their molecular partners and regulatory networks may differ substantially.

Recent evidence suggests that various signals can trigger the overexpression of LINC00313. For example, TGF-β was found to induce LINC00313 in cholangiocarcinoma [28]. Additionally, the SP1 protein, a member of the Sp/KLF family of transcription factors [29], was reported to increase the expression of LINC00313 in papillary thyroid

Fig. 6 MITF overexpression counteracts the effect of miR-320b mimic in HuCCT1 cells. HuCCT1 cells were transfected with miR-NC, miR-320b mimic, miR-320b mimic + empty vector or miR-320b mimic + MITF expression vector. **A** WB analysis of MITF protein levels in each experimental group. **B** CCK-8 proliferation assay, **C** Wound healing migration assay, **D** Transwell invasion assay, **E** RT-qPCR detection of N-cadherin, Vimentin, MMP1, MMP2, and MMP9, **F** Apoptosis detection by flow cytometry, and **G** WB analysis of apoptosis-related proteins (Bax, cleaved caspase-3, and Bcl-2) in each experimental condition. n = 3 independent experiments. *$p < 0.05$; **$p < 0.01$; ***$p < 0.001$; ****$p < 0.0001$

cancer [30]. However, these findings need to be validated in animal study and clinical samples to further confirm the mechanisms by which LINC00313 becomes deregulated in cancerous cells.

We identified miR-320b as a miRNA target of LINC00313, and it was downregulated in cholangiocarcinoma. This seems to be consistent with a previous study of miRNA profiling in human intrahepatic cholangiocarcinoma [31]. miR-320b overexpression suppressed malignant features of cholangiocarcinoma cells. In agreement with our findings, miR-320b has been found to inhibit the angiogenesis and tumor growth in lung cancer [32]. Furthermore, miR-320b suppresses the cell proliferation by repressing the expression of proto-oncogene c-Myc in colon cancer [33], while in pancreatic cancer, it downregulates FOXM1 to impede cancer cell growth [34]. These findings collectively support the tumor-suppressive function of miR-320b, positioning it as a potential anti-oncogenic target for cancer therapy [35]. Our study highlighted LINC00313 as a negative regulator of miR-320b in cholangiocarcinoma. Other recent studies have also identified lncRNAs like NR2F2-AS1 and DLEU1 as regulators of miR-320b in different cancer types [36, 37], suggesting that miR-320b may play a central role in a complex network of non-coding RNAs.

Melanocyte inducing transcription factor (MITF) was initially identified as a key transcription factor involved in the development and differentiation of melanocytes [38]. Gene mutations in MITF have been detected in melanoma patients [39], leading to changes in MITF expression and activity in melanoma cells [40]. MITF exhibits varying functions in different types of cancer. For example, in non-small cell lung cancer, MITF has been shown to act as a tumor suppressor by decreasing the expression of tumor-promoting genes [41]. Conversely, in melanoma and clear cell renal cell carcinoma, increased MITF expression has been linked to the progression of malignancy [42–44]. Previous studies in melanoma have demonstrated that MITF modulates therapeutic resistance through EGFR signaling pathways [45]. Further research has revealed that dual targeting of Aurora kinase A (AURKA) and MAPK pathways effectively overcomes MITF-mediated drug resistance in melanoma cells, suggesting the therapeutic potential of targeting these pathways [46]. Our findings support the idea that MITF promotes tumor growth, as overexpression of MITF counteracted the tumor-suppressive effects of miR-320b in cholangiocarcinoma cells. MITF may also affect drug resistance in cholangiocarcinoma cells through similar manners; however, further research is needed to fully understand the mechanisms by which MITF contributes to the aggressive behavior of cholangiocarcinoma cells.

Although our study provides insights into the functional role of the LINC00313/miR-320b/MITF axis in promoting cholangiocarcinoma aggressiveness, there are some limitations to be considered. The mechanistic investigations were mainly conducted in the HuCCT1 cell line, and evaluating the findings in additional cholangiocarcinoma cell lines or patient-derived organoids would further strengthen the conclusions. Additionally, while in vivo xenograft experiments supported the role of LINC00313 in tumorigenesis, more clinical samples should be collected to evaluate the prognostic value of LINC00313. In terms of future directions, exploring the upstream regulators that govern LINC00313 expression could elucidate potential therapeutic targets for modulating this oncogenic pathway. Furthermore, a comprehensive mechanistic understanding of how MITF drives cellular processes like proliferation, migration, and invasion in cholangiocarcinoma cells would be valuable. LINC00313 may also modulate other downstream targets to impinge on the malignancy of cholangiocarcinoma cells. Ultimately, unraveling the intricate LINC00313-mediated regulatory networks may pave the way for developing novel prognostic biomarkers and targeted therapies for this aggressive malignancy.

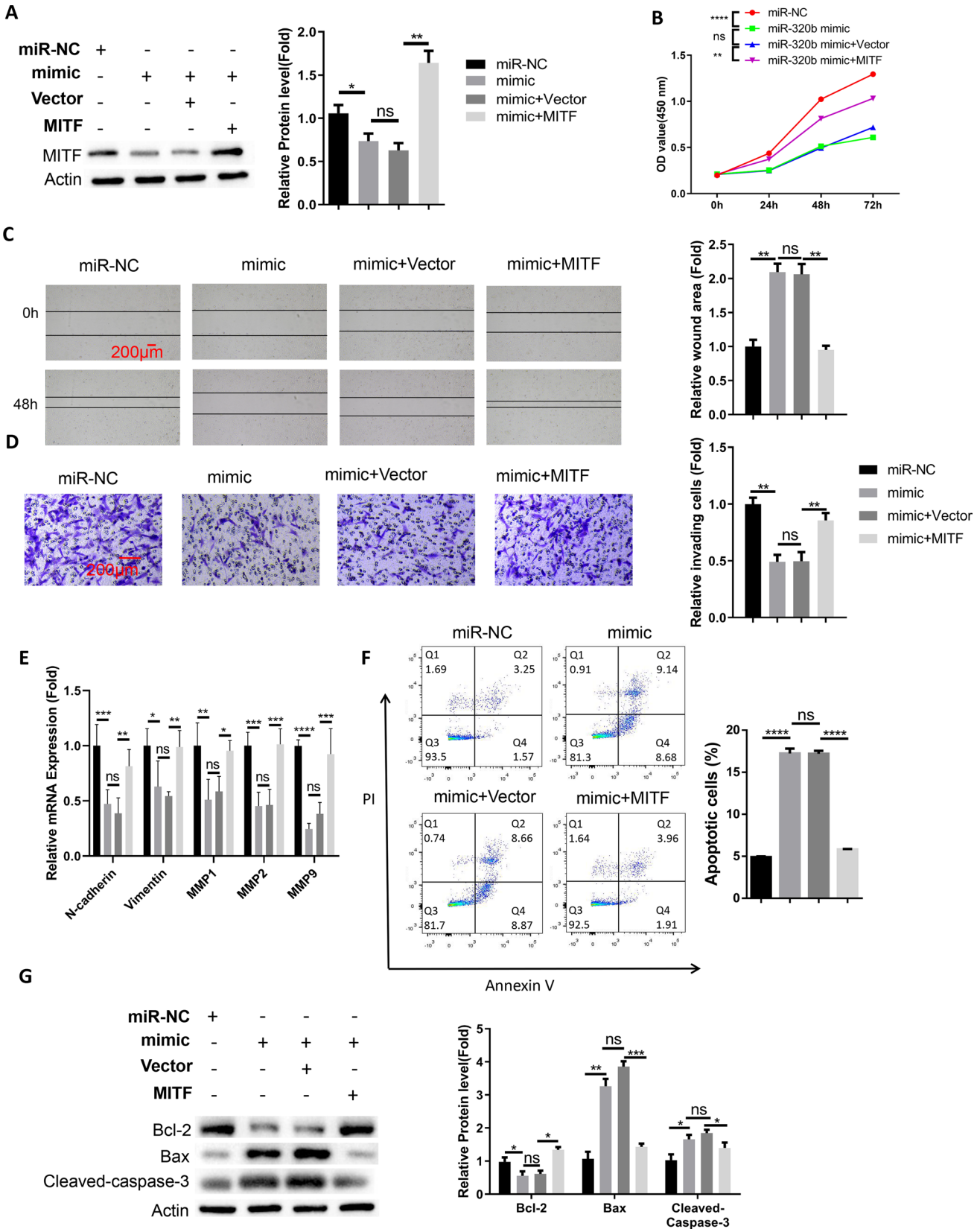
A
miR-NC + - - -
mimic - + + +
Vector - - + -
MITF - - - +
MITF
Actin
Relative Protein level(Fold)
miR-NC
mimic
mimic+Vector
mimic+MITF
B
miR-NC
miR-320b mimic
miR-320b mimic+Vector
miR-320b mimic+MITF
OD value(450 nm)
0h
24h
48h
72h
C
miR-NC
mimic
mimic+Vector
mimic+MITF
0h
48h
200μm
Relative wound area (Fold)
D
miR-NC
mimic
mimic+Vector
mimic+MITF
200μm
Relative invading cells (Fold)
E
Relative mRNA Expression (Fold)
N-cadherin
Vimentin
MMP1
MMP2
MMP9
F
miR-NC
mimic
mimic+Vector
mimic+MITF
PI
Annexin V
Q1 1.69
Q2 3.25
Q3 93.5
Q4 1.57
Q1 0.91
Q2 9.14
Q3 81.3
Q4 8.68
Q1 0.74
Q2 8.66
Q3 81.7
Q4 8.87
Q1 1.64
Q2 3.96
Q3 92.5
Q4 1.91
Apoptotic cells (%)
G
miR-NC + - - -
mimic - + + +
Vector - - + -
MITF - - - +
Bcl-2
Bax
Cleaved-caspase-3
Actin
Relative Protein level(Fold)
Bcl-2
Bax
Cleaved-Caspase-3

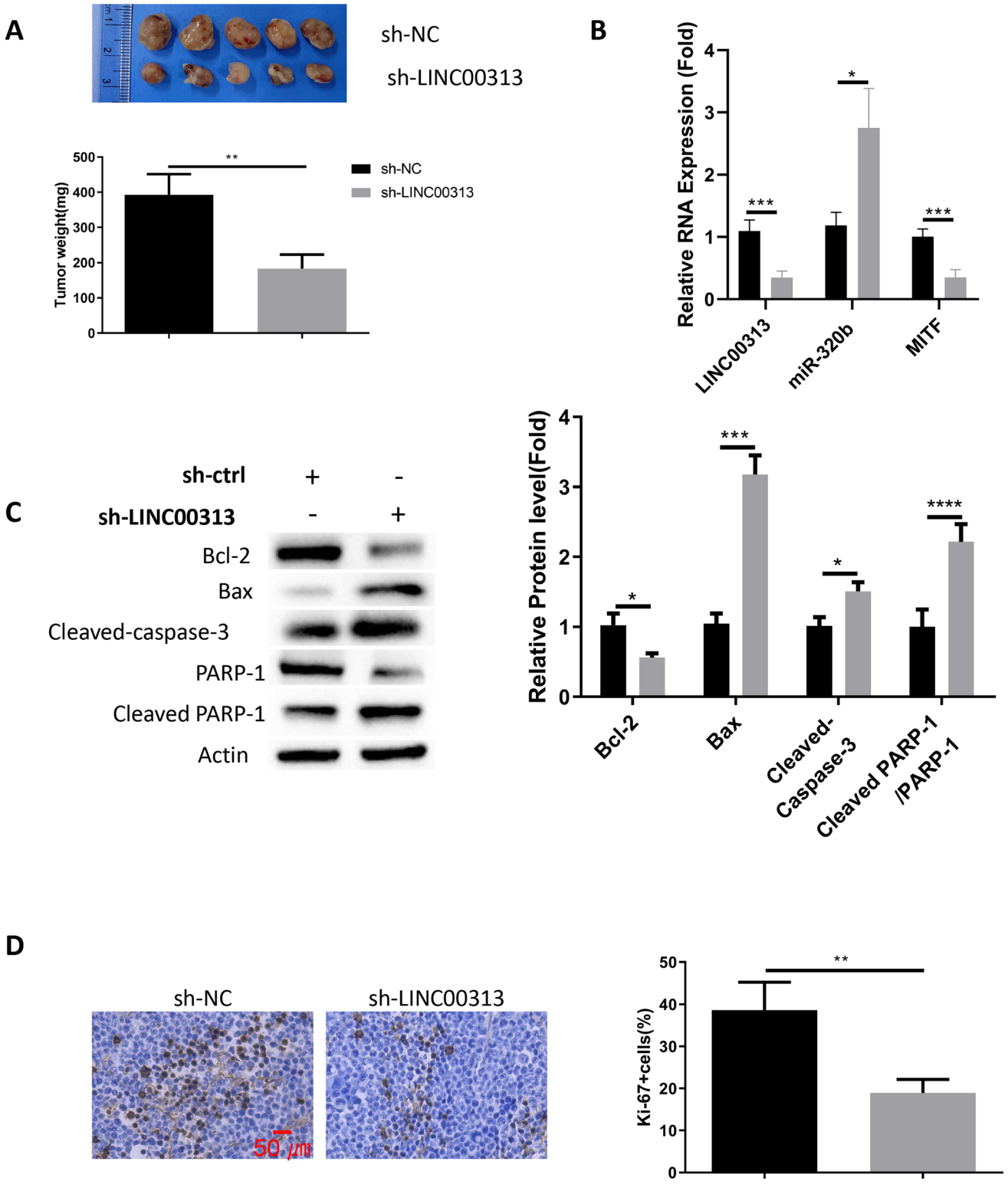

Fig. 7 LINC00313 silencing impairs the tumor formation of HuCCT1 cells in nude mice. HuCCT1 cells carrying control shRNA or the cells carrying LINC00313 shRNA were injected into nude mice (n = 5 animals in each group). **A** The tumorigenesis of HuCCT1 cells was shown in the xenobgraft tumor images and the tumor weight was summarized. **B** RT-qPCR analysis of LINC00313, miR-320b and MITF in the tumor samples. **C** WB analysis of apoptosis-related factors (Bax, cleaved caspase-3, and Bcl-2, PARP-1, Cleaved PARP-1) in the tumor samples. **D** IHC staining of the cell proliferation marker (Ki-67) in the tumor tissue sections. n = 5 animals in each group. *$p < 0.05$; **$p < 0.01$; ***$p < 0.001$; ****$p < 0.0001$

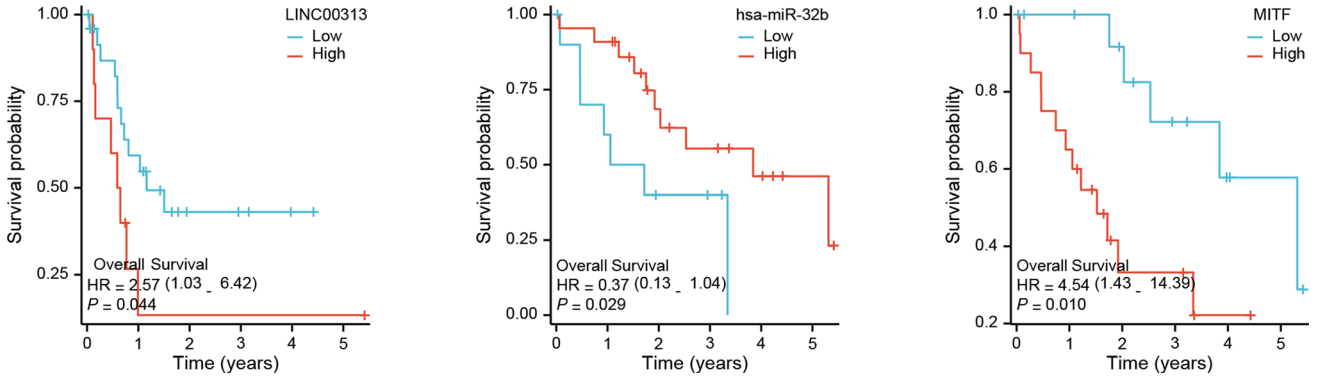

Fig. 8 The LINC00313/miR-320b/MITF axis correlates with cholangiocarcinoma patient survival. Kaplan–Meier survival curves showing the correlation between overall survival and the expression levels of LINC00313, miR-320b, and MITF in cholangiocarcinoma patients from TCGA database. The patients were divided into high and low expression groups based on the median expression value

5 Conclusion

This study establishes LINC00313 as a key oncogenic factor in cholangiocarcinoma progression, operating through a newly identified LINC00313/miR-320b/MITF regulatory axis. Our findings reveal that targeting LINC00313 could represent a promising therapeutic strategy for cholangiocarcinoma treatment. To translate these findings into therapeutic applications, future studies should focus on: (1) validating these findings in larger patient cohorts, (2) investigating MITF downstream targets, and (3) developing specific delivery methods and molecular tools (such as antisense oligonucleotides, siRNAs, or CRISPR-based approaches) for effectively targeting LINC00313 in cholangiocarcinoma cells.

Acknowledgements Not applicable.

Author contributions These should be presented as follows: Yan Jin designed the research study. Jing Xu, Tingqiu Wan performed the research. Yunjin Ya, Xi Li provided help and advice. Xi Wang analyzed the data. Ziyu Wang and Jiao Li wrote the manuscript. All authors contributed to editorial changes in the manuscript. All authors read and approved the final manuscript.

Funding This research was funded by Ten Thousand People Program—Famous Doctor Special.

Data availability The data generated in this study are available upon request to the corresponding author.

Declarations

Ethics approval and consent to participate The use of human samples gained the approval of the Medical Ethics Committee of First People's Hospital of Yunnan Province (KHLL2024-KY227). All the recruited subjects signed the written informed consent. All the sample handling and data processing steps were following the Declaration of Helsinki. Animal protocols were in compliance with the guidelines of animal care and welfare and were approved by the Experimental Animal Ethics Committee of Yunnan Besta Biotechnology Co. LTD. (BST-MICE-20221229-02).

Consent for publication All authors are aware of and have consented to publication.

Competing interests The authors declare no competing interests.

References

1. Vogel A, Wege H, Caca K, Nashan B, Neumann U. The diagnosis and treatment of cholangiocarcinoma. Dtsch Arztebl Int. 2014;111(44):748–54.
2. Zheng Q, Zhang B, Li C, Zhang X. Overcome drug resistance in cholangiocarcinoma: new insight into mechanisms and refining the preclinical experiment models. Front Oncol. 2022;17(12): 850732.
3. Sitthirak S, Suksawat M, Phetcharaburanin J, Wangwiwatsin A, Klanrit P, Namwat N, Khuntikeo N, Titapun A, Jarearnrat A, Sangkhamanon S, Loilome W. Chemotherapeutic resistant cholangiocarcinoma displayed distinct intratumoral microbial composition and metabolic profiles. PeerJ. 2022;16(10): e13876.
4. Jang JY, Kim SW, Park DJ, Ahn YJ, Yoon YS, Choi MG, Suh KS, Lee KU, Park YH. Actual long-term outcome of extrahepatic bile duct cancer after surgical resection. Ann Surg. 2005;241(1):77–84.
5. Elgenidy A, Afifi AM, Jalal PK. Survival and causes of death among patients with intrahepatic cholangiocarcinoma in the united states from 2000 to 2018. Cancer Epidemiol Biomarkers Prev. 2022;31(12):2169–76.
6. Bertuccio P, Malvezzi M, Carioli G, Hashim D, Boffetta P, El-Serag HB, La Vecchia C, Negri E. Global trends in mortality from intrahepatic and extrahepatic cholangiocarcinoma. J Hepatol. 2019;71(1):104–14.
7. Wu L, Tsilimigras DI, Paredes AZ, Mehta R, Hyer JM, Merath K, Sahara K, Bagante F, Beal EW, Shen F, Pawlik TM. Trends in the incidence, treatment and outcomes of patients with intrahepatic cholangiocarcinoma in the USA: facility type is associated with margin status, use of lymphadenectomy and overall survival. World J Surg. 2019;43(7):1777–87.
8. Zhao M, Feng J, Tang L. Competing endogenous RNAs in lung cancer. Cancer Biol Med. 2021;18(1):1–20.
9. Qu J, Li M, Zhong W, Hu C. Competing endogenous RNA in cancer: a new pattern of gene expression regulation. Int J Clin Exp Med. 2015;8(10):17110–6.
10. Nandwani A, Rathore S, Datta M. LncRNAs in cancer: regulatory and therapeutic implications. Cancer Lett. 2021;31(501):162–71.
11. Qian Y, Shi L, Luo Z. Long non-coding RNAs in cancer: implications for diagnosis, prognosis, and therapy. Front Med (Lausanne). 2020;30(7): 612393.
12. Peng H, Lu M, Selaru FM. The genome-wide gene expression profiling to predict competitive endogenous RNA network in hepatocellular cancer. Genom Data. 2015;7(4):93–5.
13. Zhou M, Diao Z, Yue X, Chen Y, Zhao H, Cheng L, Sun J. Construction and analysis of dysregulated lncRNA-associated ceRNA network identified novel lncRNA biomarkers for early diagnosis of human pancreatic cancer. Oncotarget. 2016;7(35):56383–94.
14. Arun K, Arunkumar G, Bennet D, Chandramohan SM, Murugan AK, Munirajan AK. Comprehensive analysis of aberrantly expressed lncRNAs and construction of ceRNA network in gastric cancer. Oncotarget. 2018;9(26):18386–99.
15. Zhou X, Liu J, Wang W. Construction and investigation of breast-cancer-specific ceRNA network based on the mRNA and miRNA expression data. IET Syst Biol. 2014;8(3):96–103.
16. Shi X, Zhang H, Wang M, Xu X, Zhao Y, He R, Zhang M, Zhou M, Li X, Peng F, Shi C, Shen M, Wang X, Guo X, Qin R. LncRNA AFAP1-AS1 promotes growth and metastasis of cholangiocarcinoma cells. Oncotarget. 2017;8(35):58394–404.
17. Zhang S, Xiao J, Chai Y, Du YY, Liu Z, Huang K, Zhou X, Zhou W. LncRNA-CCAT1 promotes migration, invasion, and EMT in intrahepatic cholangiocarcinoma through suppressing miR-152. Dig Dis Sci. 2017;62(11):3050–8.
18. Sun ZP, Tan ZG, Peng C, Yi WM. LncRNA SNHG3 facilitates the malignant phenotype of cholangiocarcinoma cells via the miR-3173-5p/ERG axis. J Gastrointest Surg. 2022;26(4):802–12.
19. Yu Y, Chen Q, Zhang X, Yang J, Lin K, Ji C, Xu A, Yang L, Miao L. Long noncoding RNA ANRIL promotes the malignant progression of cholangiocarcinoma by epigenetically repressing ERRFI1 expression. Cancer Sci. 2020;111(7):2297–309.
20. Xu F, Zhao Y, Qin G, Huan Y, Li L, Gao W. Comprehensive analysis of competing endogenous RNA networks associated with cholangiocarcinoma. Exp Ther Med. 2019;18(5):4103–12.
21. Song W, Miao DL, Chen L. Comprehensive analysis of long noncoding RNA-associated competing endogenous RNA network in cholangiocarcinoma. Biochem Biophys Res Commun. 2018;506(4):1004–12.
22. Liu Z, Fang B, Cao J, Zhou Q, Zhu F, Fan L, Xue L, Huang C, Bo H. LINC00313 regulates the metastasis of testicular germ cell tumors through epithelial-mesenchyme transition and immune pathways. Bioengineered. 2022;13(5):12141–55.
23. Zhai Y, Liu Y, Wang Z, Wang W, Zhou J, Lu J. Long non-coding RNA LINC00313 accelerates cervical carcinoma progression by miR-4677-3p/CDK6 axis. Onco Targets Ther. 2021;29(14):2213–26.
24. Xing CY, Zhang YZ, Hu W, Zhao LY. LINC00313 facilitates osteosarcoma carcinogenesis and metastasis through enhancing EZH2 mRNA stability and EZH2-mediated silence of PTEN expression. Cell Mol Life Sci. 2022;79(7):382.
25. Kong W, Zhang L, Chen Y, Yu Z, Zhao Z. Cancer cell-derived exosomal LINC00313 induces M2 macrophage differentiation in non-small cell lung cancer. Clin Transl Oncol. 2022;24(12):2395–408.
26. Chen H, Wahafu P, Wang L, Chen X. LncRNA LINC00313 knockdown inhibits tumorigenesis and metastasis in human osteosarcoma by upregulating FOSL2 through sponging miR-342-3p. Yonsei Med J. 2020;61(5):359–70.
27. He W, Lin X. LINC00313 promotes the proliferation and inhibits the apoptosis of chondrocytes via regulating miR-525-5p/GDF5 axis. J Orthop Surg Res. 2023;18(1):137.
28. Papoutsoglou P, Louis C, Pineau R, L'Haridon A, Banales JM, Gilot D, Aubry M, Coulouarn C. TGFβ-induced long non-coding RNA LINC00313 activates Wnt signalling and promotes cholangiocarcinoma. bioRxiv 2022.09.28.509889.
29. O'Connor L, Gilmour J, Bonifer C. the role of the ubiquitously expressed transcription factor Sp1 in tissue-specific transcriptional regulation and in disease. Yale J Biol Med. 2016;89(4):513–25.
30. Yan DG, Liu N, Chao M, Tu YY, Liu WS. SP1-induced upregulation of long noncoding RNA LINC00313 contributes to papillary thyroid cancer progression via the miR-422a. Eur Rev Med Pharmacol Sci. 2019;23(3):1134–44.
31. Chen L, Yan HX, Yang W, Hu L, Yu LX, Liu Q, Li L, Huang DD, Ding J, Shen F, Zhou WP, Wu MC, Wang HY. The role of microRNA expression pattern in human intrahepatic cholangiocarcinoma. J Hepatol. 2009;50(2):358–69.

32. Ma YS, Shi BW, Guo JH, Liu JB, Yang XL, Xin R, Shi Y, Zhang DD, Lu GX, Jia CY, Wang HM, Wang PY, Yang HQ, Zhang JJ, Wu W, Cao PS, Yin YZ, Gu LP, Tian LL, Lv ZW, Wu CY, Wang GR, Yu F, Hou LK, Jiang GX, Fu D. microRNA-320b suppresses HNF4G and IGF2BP2 expression to inhibit angiogenesis and tumor growth of lung cancer. Carcinogenesis. 2021;42(5):762–71.
33. Wang H, Cao F, Li X, Miao H, E J, Xing J, Fu CG. miR-320b suppresses cell proliferation by targeting c-Myc in human colorectal cancer cells. BMC Cancer. 2015;15:748.
34. Jingyang Z, Jinhui C, Lu X, Weizhong Y, Yunjiu L, Haihong W, Wuyuan Z. Mir-320b inhibits pancreatic cancer cell proliferation by targeting FOXM1. Curr Pharm Biotechnol. 2021;22(8):1106–13.
35. Liang Y, Li S, Tang L. MicroRNA 320, an anti-oncogene target miRNA for cancer therapy. Biomedicines. 2021;9(6):591.
36. Luo M, Deng S, Han T, Ou Y, Hu Y. LncRNA NR2F2-AS1 functions as a tumor suppressor in gastric cancer through targeting miR-320b/PDCD4 pathway. Histol Histopathol. 2022;37(6):575–85.
37. Xu D, Yang F, Fan Y, Jing W, Wen J, Miao W, Ding X, Yang H. LncRNA DLEU1 contributes to the growth and invasion of colorectal cancer via targeting miR-320b/PRPS1. Front Oncol. 2021;25(11): 640276.
38. Kawakami A, Fisher DE. The master role of microphthalmia-associated transcription factor in melanocyte and melanoma biology. Lab Invest. 2017;97(6):649–56.
39. Guhan SM, Artomov M, McCormick S, Njauw C, Stratigos AJ, Shannon K, Ellisen LW, Tsao H. Cancer risks associated with the germline MITF(E318K) variant. Sci Rep. 2020;10(1):17051.
40. Hartman ML, Czyz M. MITF in melanoma: mechanisms behind its expression and activity. Cell Mol Life Sci. 2015;72(7):1249–60.
41. Hsiao YJ, Chang WH, Chen HY, Hsu YC, Chiu SC, Chiang CC, Chang GC, Chen YJ, Wang CY, Chen YM, Lin CY, Chen YJ, Yang PC, Chen JJW, Yu SL. MITF functions as a tumor suppressor in non-small cell lung cancer beyond the canonically oncogenic role. Aging (Albany). 2020;13(1):646–74.
42. Wellbrock C, Marais R. Elevated expression of MITF counteracts B-RAF-stimulated melanocyte and melanoma cell proliferation. J Cell Biol. 2005;170(5):703–8.
43. Kim N, Kim S, Lee MW, Jeon HJ, Ryu H, Kim JM, Lee HJ. MITF promotes cell growth, migration and invasion in clear cell renal cell carcinoma by activating the RhoA/YAP signal pathway. Cancers (Basel). 2021;13(12):2920.
44. Dilshat R, Fock V, Kenny C, Gerritsen I, Lasseur RMJ, Travnickova J, Eichhoff OM, Cerny P, Möller K, Sigurbjörnsdóttir S, Kirty K, Einarsdottir BÓ, Cheng PF, Levesque M, Cornell RA, Patton EE, Larue L, de Tayrac M, Magnúsdóttir E, Ögmundsdóttir MH, Steingrimsson E. MITF reprograms the extracellular matrix and focal adhesion in melanoma. Elife. 2021;13(10): e63093.
45. Ji Z, Erin Chen Y, Kumar R, Taylor M, Jenny Njauw CN, Miao B, Frederick DT, Wargo JA, Flaherty KT, Jönsson G, Tsao H. MITF modulates therapeutic resistance through EGFR signaling. J Invest Dermatol. 2015;135(7):1863–72.
46. Pathria G, Garg B, Borgdorff V, Garg K, Wagner C, Superti-Furga G, Wagner SN. Overcoming MITF-conferred drug resistance through dual AURKA/MAPK targeting in human melanoma cells. Cell Death Dis. 2016;7(3): e2135.